

The INTEGRAL view of Gamma-Ray Bursts

P. Ubertini*, A. Corsi^{*,†}, S. Foley^{**}, S. McGlynn[‡], G. De Cesare* and A. Bazzano*
on behalf of the IBIS Team

*IASF-Roma, INAF, Via Fosso del Cavaliere, 100 - 00133 Roma, Italy

†Università di Roma "Sapienza", Piazzale Aldo Moro 2 - 00185 Roma, Italy

**UCD School of Physics, University College Dublin, Dublin 4, Ireland

‡Department of Physics, Royal Institute of Technology (KTH), AlbaNova, SE-106 91 Stockholm, Sweden

Abstract. After more than six and half years in orbit, the ESA space observatory INTEGRAL has provided new, exciting results in the soft gamma-ray energy range (from a few keV to a few MeV). With the discovery of about 700 hard X-Ray sources, it has changed our previous view of a sky composed of peculiar and "monster" sources. The new high energy sky is in fact full of a large variety of normal, very energetic emitters, characterized by new accretion and acceleration processes (see also IBIS cat4 [1]). If compared to previous IBIS/ISGRI surveys it is clear that there is a continual increase in the rate of discoveries of HMXB and AGN, including a variety of distant QSOs. This is basically due to increased exposure away from the Galactic Plane, while the percentage of sources without an identification has remained constant. At the same time, about one GRB/month is detected and imaged by the two main gamma-ray instruments on board: IBIS and SPI. INTEGRAL, after six and half years of observations, has completed the Core Programme phase and is now fully open to the scientific community for Open Time and Key Programme observations, with AO7 recently announced by ESA.

In this paper we review the major achievements of the INTEGRAL Observatory in the field of Gamma Ray Bursts.

Keywords: γ -rays, GRB, surveys

PACS: 95.85.Pw γ -ray; 98.70.Rz γ -ray sources; γ -ray bursts; 95.80.+p sky surveys; 95.55.Ka X- and γ -ray telescopes and instrumentation; 95.30.Gv Radiation mechanisms; polarization

THE INTEGRAL OBSERVATORY

The ESA INTEGRAL (International Gamma-Ray Astrophysics Laboratory) observatory was selected in June 1993 as the next medium-size scientific mission within the ESA Horizon 2000 programme. INTEGRAL [2], is dedicated to the fine spectroscopy (2.5 keV FWHM @ 1 MeV) and fine imaging (angular resolution: 12 arcmin FWHM) of celestial gamma-ray sources in the energy range 15 keV to 10 MeV. While the imaging is carried out by the imager IBIS [3], the fine spectroscopy is performed by the spectrometer SPI [4] and coaxial monitoring capability in the X-ray (3-35 keV) and optical (V-band, 550 nm) energy ranges is provided by the JEM X and OMC instruments [5, 6]. SPI, IBIS and Jem-X, the spectrometer, imager and X-ray monitor, are based on the use of the coded aperture mask technique, which is a key method used to provide images at energies above tens of keV, where photon focusing becomes impossible using standard grazing techniques. Moreover, coded masks optimise background subtraction capability because of the opportunity to observe the source and the off-source sky at the same time. This is achieved simultaneously for all the sources present in the telescope field of view. In fact, for any particular source direction, the detector pixels are divided into two sets: those capable of viewing the source and those for which the flux is blocked

by opaque tungsten mask elements. This very well established technique is discussed in detail by [7] and is extremely effective in controlling the systematic error in all telescope observations, working remarkably well for weak extragalactic field sources as well as for crowded galactic regions, such as our Galactic Center. The mission was conceived from the beginning as an observatory led by ESA with contributions from Russia (PROTON launcher) and NASA (Deep Space Network ground station). INTEGRAL was launched from Baikonur on October 17th, 2002 and inserted into an highly eccentric orbit (characterized by 9000 km perigee and 154000 km apogee). The high perigee was used in order to provide long uninterrupted observations with nearly constant background and away from the electron and proton radiation belts. Scientific observations can then be carried out while the satellite is above a nominal altitude of 60000 km while entering the radiation belts, and above 40000 km while leaving them. This strategic choice ensures that about 90% of the time is used for scientific observations with a data rate of realtime 108 kbps science telemetry being received from the ESA station at Redu and NASA station at Goldstone. The data are received by the INTEGRAL Mission Operation Centre (MOC) in Darmstadt (Germany) and relayed to the Science Data Center (ISDC, [8]) which provides the final consolidated data products to the observers and later archives them for

public use. The proprietary data become public one year after their distribution to single observation PIs.

To date INTEGRAL has already carried out more than 6 years of Core, Key and Guest Observer Programme observations in the energy range from 5 keV up to 10 MeV with high angular resolution (few arcmin PSLA of the IBIS imager) and excellent spectral capability (2.5 keV spectral resolution of the SPI germanium spectrometer).

HIGHLIGHTS FROM THE INTEGRAL GRB SAMPLE

The 1st bursts in the sample

GRB 021125

Just a few weeks after its launch, INTEGRAL started an in-orbit calibration observing Cyg X-1. On November 25th, 2002, the satellite was set up for a special observation with the PICsIT layer in the non-standard photon-by-photon mode [9]. Since PICsIT operates in an energy band where the background rate is very high, to perform the calibration it was necessary to limit the operative range below 500 keV and to strongly reduce the telemetry allocation to the other instruments (SPI, JEM-X, OMC were sending only housekeeping data to ground) and to the ISGRI layer of IBIS. During this test, at 17:58:30 UTC a GRB occurred in the partially coded field of view of IBIS (about 7.3° off-axis) and lasted about 24 s [10, 11]. The burst was soon confirmed by the Inter Planetary Network (IPN, [12]). GRB 021125 was the first GRB detected by INTEGRAL in the field of view of the IBIS imager. The sky coordinates reconstructed with IBIS and SPI were in agreement with each other, and consistent with the IPN error box. The spectrum and light curve, obtained using independent methods, yielded consistent results. GRB 021125 thus proved the capabilities of the instruments on board the INTEGRAL satellite for GRB observations.

GRB 030131

Although not specifically designed as a GRB-oriented mission, INTEGRAL has contributed to the rapid localization of GRBs thanks to the INTEGRAL Burst Alert System (IBAS, [13]). This software, running at the ISDC [8], is able to detect and localize GRBs with a precision of a few arcminutes in a few seconds, and to distribute their coordinates in near real time over the Internet. In addition, the high sensitivity of the INTEGRAL instruments is particularly well-suited to study in detail the prompt γ -ray emission of the faintest bursts. On January

31 2003 at 07:38:49 UTC, GRB 030131 was detected in the field of view of IBIS and SPI. The IBIS/ISGRI time-resolved spectroscopy of the burst [14] was consistent with the overall hard-to-soft evolution observed by BATSE in brighter GRBs [15, 16]. However, the fluence of GRB 030131 was an order of magnitude smaller, indicating that such spectral behavior also applied to fainter GRBs. Clear evidence of such behavior was also reported for bursts studied with BeppoSAX in the 2-700 keV energy range (e.g. [17]).

From extremely hard to soft bursts

GRB 030406

ISGRI and PICsIT can act as a Compton telescope, registering photons that are scattered in one and absorbed in the other detector. The coincidence time window is a parameter programmable on-board and the mode is sensitive between 200 keV and ~ 3 MeV. Thanks to the Compton mode data, INTEGRAL has been able to make successful, independent burst localizations, as in the case of GRB 030406 ([18] and references therein). GRB 030406 was detected by SPI-ACS on-board INTEGRAL as well as by Ulysses, Konus, and Mars Odyssey [19]. It was a long burst lasting ~ 65 s. Ulysses reported a fluence of 1.3×10^{-5} erg cm $^{-2}$ s $^{-1}$ (25-100 keV). In the 50 keV - 3 MeV energy range, a fit to the spectrum of the burst peak (2.8 s around the maximum) with a broken power law, revealed that the peak was very hard. Below 400 keV, the νF_ν spectrum increased with index $\sim +3.5$, and above this energy the index was still positive and equal to $\sim +0.3$ [18]. Compared to the distribution of the low and high energy spectral indices of the sample of 156 bright BATSE bursts presented by [20], both the low and the high energy spectral indices of GRB 030406 would lie in the upper tails of the corresponding distributions in this BATSE sample. Its spectrum was thus in clear contradiction with the synchrotron model of GRBs [21, 22], which predicts that there is a strict upper limit on the low energy spectral index of $-2/3$ [15]. The low energy spectral slope of the burst was instead consistent within the error bars with the jitter radiation model of GRBs [23]. [24] also showed that the low energy spectral slopes of several GRBs are indeed much larger than expected in the synchrotron model ($\sim 0.5 - 1$). Furthermore, GRB 030406 provided a hint for the existence of bursts with the peak of νF_ν spectrum, E_{peak} , above the distribution shown by [25] which truncates at ~ 1 MeV for the bright BATSE bursts. An $E_{peak} > 1.1$ MeV, as estimated for GRB 030406 (90% lower limit), is also on the high end of the Amati (and Ghirlanda) relation [26, 27]. According to such a relation, the estimated isotropic ra-

diated energy is larger than $(6 - 20) \times 10^{53}$ ergs, where the uncertainty stems from the inaccuracy of the Amati relation [18]. GRB 030406 thus showed that hard bursts are very energetic. In summary, GRB 030406 confirmed that INTEGRAL in the Compton mode can detect hard GRBs, with a localization accuracy of a few degrees [18]. The GRB spectra can be studied in the range from ~ 200 keV to ~ 3 MeV depending on the location of the burst in the instrument coordinates.

XRF 040812

In addition to very hard bursts, INTEGRAL has also yielded interesting results on much softer GRBs, as for the case of the X-Ray Flash (XRF) 040812. XRF 040812 was discovered by INTEGRAL on 2004 August 12.251 UT, with the IBIS/ISGRI instrument in the 15-200 keV band ([28] and Fig. 1). A spectral analysis of the burst revealed good agreement with a Band model [29], with low energy photon index $\alpha = -1$ and high energy photon index $\beta = -3$. The νF_ν spectrum peaked at an energy $E_{peak} \sim 27$ keV (see Fig. 2), and the 20-200 keV flux was measured to be $F_{20-200\text{keV}} \sim 2.2 \times 10^{-8}$ ergs cm^{-2} s^{-1} . Two epochs of Chandra observations (5 and 10 days after the burst) revealed the presence of a fading, uncatalogued source within the INTEGRAL error box [30, 31]. Optical observations at the VLT started 0.7 days after the XRF and the monitoring continued until 220 days after [32], when the level of the host galaxy emission was reached. These observations constrained the redshift to lie in the range $0.3 < z < 0.7$ [32]. Taking into account the cosmological redshift, and using INTEGRAL data, it was possible to establish that XRF 040812 was consistent with the $E_{peak} - E_{iso}$ relation, ranking among X-Ray Rich GRBs rather than an intrinsic XRFs (see Fig. 3 and Fig. 6 in [33]).

Peculiar spectral features: Fe-line and inverse Compton emission

GRB 030227 was the first GRB for which the quick localization obtained with the IBAS has led to the discovery of X-ray and optical afterglows (see [35] and references therein). The IBAS alert message with the preliminary position of the burst was delivered to the IBAS Team at 08:42:38 UT on 2003 February 27, only 35 s after the start of the burst (most of this delay was due to buffering of the telemetry on board the satellite and to data transmission between the ground station and the ISDC). Unfortunately, the Internet message with these coordinates could not be distributed in real time. In fact, the detection of GRB 030227 occurred dur-

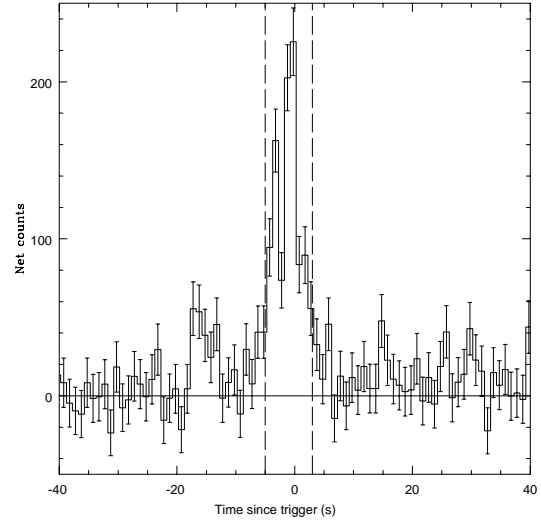


FIGURE 1. The IBIS/ISGRI 20 - 60 keV light curve of XRF 040812.

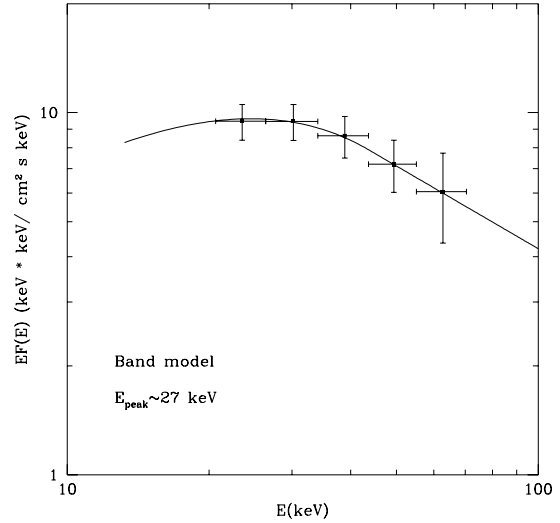


FIGURE 2. XRF 040812 spectrum: assuming a Band model [29], we get $\alpha \sim -1$ and ~ -3 for the low and high energy spectral indices of the photon spectrum, consistent with typical XRF values. The νF_ν peak energy is at $E_{peak} \sim 27$ keV.

ing a calibration observation of the Crab Nebula. Since the instrument configuration during these observations caused some spurious IBAS triggers, the automatic delivery of the alerts to external clients had been temporarily disabled. Nevertheless, this information was distributed within less than 1 hr after the GRB (at 08:42:03 UT). GRB 030227 had a duration of about 20 s, thus belonging to the class of long GRBs. Its peak flux and fluence,

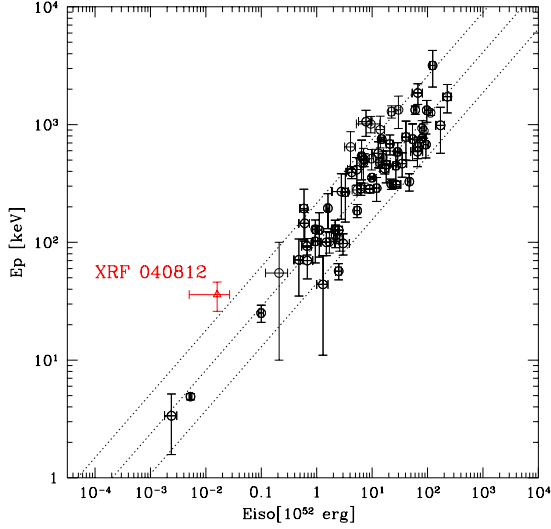


FIGURE 3. $E_{peak} - E_{iso}$ correlation for XRF 040812 compared with the 70 GRBs and XRFs with firm estimates of the redshift reported in [34]. XRF 040812 ranks among XRRs rather than intrinsic XRFs.

converted to the BATSE 50-300 keV energy range, were ~ 0.6 photons $\text{cm}^{-2} \text{s}^{-1}$ and $\sim 7 \times 10^{-7}$ ergs cm^{-2} , respectively [35]. About three-quarters of the GRBs in the fourth BATSE catalog [36] had a higher peak flux, indicating that GRB 030227 was quite faint. The burst time-averaged spectrum was fit by a single power-law with photon index 1.9 ± 0.3 . The 20-200 keV flux of the burst was measured to be 4.7×10^{-8} ergs $\text{cm}^{-2} \text{s}^{-1}$. Based on the background-subtracted count rates in the ranges 40-100 keV and 20-40 keV, both SPI and IBIS showed evidence for a hard-to-soft evolution of the burst [35].

XMM-Newton observed the position of GRB 030227 for ~ 13 hrs, starting on February 27 at 16:58 UT, about 8 hrs after the event [35]. An absorbed power-law fit to the afterglow spectrum gave an unacceptable fit. An acceptable one could be obtained by fixing N_H to the Galactic value and adding a redshifted neutral absorption, which yielded an estimated redshift of $z = 3.9 \pm 0.3$ [35]. The fit residuals suggested the presence of possible lines in the spectrum. Adding Gaussian lines at different energies and with fixed widths, smaller than the instrumental resolution, a possibly significant line was found at an observed energy of 1.67 ± 0.01 keV [35]. According to an F-test, such a line was significant at the 3.2σ level (to be

considered with caution, see [37]). If interpreted as being due to Fe, as suggested for similar features observed in other afterglows (see e.g. [38, 39, 40, 41, 42, 43, 44]), the implied redshift of $\sim 2.7 - 3$ (depending on the Fe ionization state) was consistent with the value derived from the absorption (but other interpretations in terms of lighter elements were also possible [45]).

ToO observations were triggered starting at 5.3 hrs with different optical telescopes [46]. The spectral flux distribution of the optical afterglow of GRB 030227 on 28.24 UT Feb 2003, determined by means of the broadband photometric measurements obtained with the different telescopes, gave a NIR/optical spectral index of $\beta_{opt-NIR} = -1.25 \pm 0.14$, consistent with the spectral index for the unabsorbed X-ray spectrum ($\beta_X = -0.94 \pm 0.05$, [35]). However, the NIR/optical and X-ray spectra did not match each other's extrapolations, similarly to other previously and more recently observed GRBs [47, 48, 49]. Considerable extinction in the host galaxy (considering different extinction laws) could not explain such an effect [46]. Thus, it was suggested that in contrast to the NIR/optical band, where synchrotron processes dominate, an important contribution of inverse Compton scattering was present in the X-ray spectrum, besides line emission [35, 45]. This implied a lower limit on the density of the external medium of $n > 10 \text{ cm}^{-3}$ [46].

A low-luminosity, nearby GRB

GRB 031203 was detected by IBIS on December 3, 2003 at 22:01:28 UTC. The light curve in Fig. 4 a shows a single pulse with a duration of ~ 40 s. The spectrum was also typical for a long-duration GRB and was well fit by a single power-law model that constrained $E_{peak} > 190$ keV [50]. GRB 031203 is the fourth nearest GRB detected to date at a redshift of $z = 0.1055$ and is notable for its unambiguous spatial and temporal association with the supernova SN 2003lw. It is a confirmed low-luminosity GRB with an isotropic energy of $\sim 4 \times 10^{49}$ erg (20-200 keV). GRB 980425, with an isotropic energy release of $\sim 10^{48}$ erg was the first such under-luminous GRB to be detected and was associated with the nearby ($z = 0.0085$) SN 1998bw. Both GRB 980425 and GRB 031203 violate the Amati correlation between isotropic energy, E_{iso} and peak energy, E_{peak} , that would predict $E_{peak} < 10$ keV [51]. These GRBs are clearly sub-energetic in the γ -ray band, and their proximity (and hence implied abundance) makes it of great interest to understand their origin and relation to the more distant cosmological GRBs.

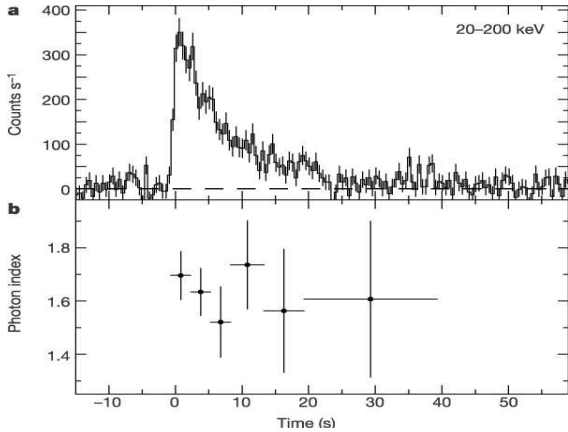


FIGURE 4. **a)** Lightcurve of GRB 031203 in the 20–200 keV energy band in 0.5 s time bins. **b)** The evolution of the photon index throughout the duration of the burst. There is no evidence for significant spectral evolution on short timescales. Credit: Sazonov et al. [50].

Polarisation studies

Linear polarisation in GRB prompt emission is an important diagnostic with the potential to significantly constrain GRB emission models (see e.g. [52] and references therein for a recent discussion of this topic). GRB 041219a is the most intense burst localised by INTEGRAL with a fluence of 5.7×10^{-4} ergs cm^{-2} over the energy range 20 keV - 8 MeV [53], and is an ideal candidate for such a study. GRB 041219a was detected by IBAS and ISGRI at 01:42:18 UTC on December 19th 2004 [54]. The burst was in the fully coded field of view of both ISGRI and SPI and was 3° off the X-axis, and 155° in azimuth from the Y-axis. It was also detected by the Burst Alert Telescope (BAT) on-board the *Swift* satellite [55]. A T_{90} value of 186 s (~ 20 keV - 8 MeV) was determined from the SPI light curve. The temporal structure of the burst was unusual, with an initial weak precursor pulse followed by a long quiescent time interval and the main emission beginning at ~ 250 s post trigger [56]. Although the SPI light curve is quiescent from $\sim 7 - 200$ s, emission was detected in the BAT light curve, particularly in the lower energy channels 15-25 keV and 25- 50 keV [57]. In addition, a spectrally soft pulse was detected in the All Sky Monitor (ASM) [58], beginning at 80 s in the quiescent period of the SPI observation [59].

Polarisation can be measured by INTEGRAL/SPI using multiple events scattered into adjacent detectors because the Compton scatter angle depends on the polarisation of the incoming photon. For the case of GRB 041219a, [60] found that the distribution of azimuthal scattering angles was better represented by a polarized source compared to a non-polarized source, but with low statistical significance. Using multiple-detector co-

incidence events in the 100-350 keV energy band, such analysis yielded a polarization fraction $(98 \pm 33)\%$ [60], which statistically did not allow the authors to claim a polarization detection from this source. Moreover, different event selection criteria lead to even less significant polarization fractions, e.g., lower polarization fractions were obtained when higher energies were included in the analysis [60], and the possibility that the measured modulation was dominated by instrumental systematics could not be ruled out [60].

[53] have also carried out polarisation studies on GRB 041219a, comparing the observed data to various combinations of simulated polarised and unpolarised data. The analysis was carried out dividing the scatter pairs into 6 different directions (0 - 300 degrees) and in the energy ranges 100 - 350 keV and 100 - 500 keV. The degree of linear polarisation in the GRB brightest pulse of duration 66 s (see Fig. 5) was found to be $(63^{+31}_{-30})\%$ at an angle of (70^{+14}_{-11}) degrees in the 100 - 350 keV energy range. The degree of polarisation was also constrained in the brightest 12 s of the GRB (see Fig. 5) and a polarisation fraction of $(96^{+39}_{-40})\%$ at an angle of (60^{+12}_{-14}) degrees was determined over the same energy range. However, despite extensive analysis and simulations, a systematic effect that could mimic the weak polarisation signal could not be definitively excluded. Over several energy ranges and time intervals, the results by [53] were consistent with a polarisation signal of about 60% but at a low level of significance ($\sim 2\sigma$). By fitting the azimuthal scatter angle distribution of the observed data over the 6 directions, [53] obtained results consistent with [60] in both magnitude and direction, within the limits given by the large error bars. Also, [53] agreed with the conclusions of [60] that the possibility of instrumental systematics dominating the measured effect cannot be excluded.

More recently, [61] reported on the polarization measurement of the prompt emission of GRB 041219a, performed using IBIS. Being composed of the two position sensitive detector layers ISGRI and PICsIT, IBIS can be used as a Compton polarimeter [62], thanks to the polarization dependency of the differential cross section for Compton scattering. [61] analyzed the different portions of the GRB 040219a prompt light curve, focusing on the brightest parts. More specifically, they analyzed the entire first and second peak, and then performed a time-resolved analysis composed of 36 intervals lasting 10 s, each one overlapping for 5 s with the previous one, over the whole duration of the GRB starting at 01:46:22 UT until 01:49:22 UT. No polarization signal could be found integrating over the whole first peak, with an upper limit of 4%. On the other hand, a modulated signal was seen in the second peak, corresponding to a polarization fraction of $43\% \pm 25\%$. Integrating over smaller portions of the GRB, highly polarized signals were measured. Re-

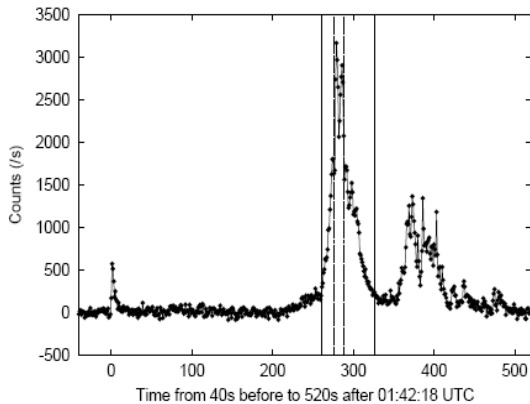


FIGURE 5. Background-subtracted single event lightcurve of GRB 041219a, summed over all SPI detectors in the energy range 20 keV - 8 MeV. The vertical solid lines mark the start and end of the 66 second emission phase ($T_0 = 261$ s to $T_0 = 327$ s). The vertical dashed lines mark the start and end of the brightest 12 seconds of the burst ($T_0 = 276$ s to $T_0 = 288$ s). T_0 is the IBAS trigger time (01:42:18UTC). Credit: McGlynn et al. 2007 [53].

sults by [61] were consistent with those by [53] for the 12 s interval on the brightest part of the GRB. However, [61] did not confirm the result by [53] on the broader 66 s time interval, where they did not detect any polarized signal.

[61] have discussed their results in the light of different emission models for GRB prompt emission: (i) Synchrotron emission from shock-accelerated electrons in a relativistic jet with an ordered magnetic field contained in the plane perpendicular to the jet velocity [63, 64, 65]; (ii) Synchrotron emission from a purely electromagnetic outflow [66]; (iii) Synchrotron emission from shock-accelerated electrons in a relativistic jet with a random field generated at the shock and contained in the plane perpendicular to the jet velocity [67, 68]; (iv) Inverse Compton emission from relativistic electrons in a jet propagating within a photon field (“Compton drag” model, [69]). Given that for the case of GRB 041219a the polarization level was varying on short timescales (reaching high values), that the polarization angle was varying as well, and that the time-averaged value over longer intervals showed reduced polarization, [61] concluded that, despite being consistent with more than one model, their results for this GRB favor synchrotron radiation from a relativistic outflow with a magnetic field, which is coherent on an angular size comparable with the angular size of the emitting region ($\sim 1/\Gamma$, scenario (i)).

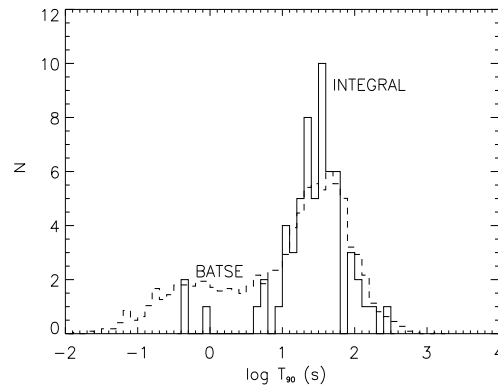


FIGURE 6. T_{90} distribution of INTEGRAL GRBs in comparison to that of BATSE (dashed line). The BATSE distribution is normalised to the INTEGRAL distribution for clarity.

GLOBAL PROPERTIES OF GRBS OBSERVED BY INTEGRAL

Duration, spectral index and peak flux distributions

The T_{90} distribution of INTEGRAL GRBs, measured in the 20–200 keV energy range, is shown in Fig. 6 and compared with the bimodal distribution obtained for BATSE GRBs [70]. There is reasonable agreement between the two distributions, especially when the small number of INTEGRAL GRBs is taken into account.

The distribution of photon indices is shown in Fig. 7 for INTEGRAL and Swift GRBs for which a power-law model was fit to the spectral data in the 20–200 keV and 15–150 keV energy ranges, respectively. In comparison to Swift, INTEGRAL detects proportionally more soft GRBs with steeper power-law photon indices.

Fig. 8 compares the peak flux distribution of the GRBs observed by IBIS to that observed by the BAT instrument on Swift. IBIS detects proportionally more weak GRBs than Swift because of its better sensitivity within a field of view that is smaller by a factor of ~ 12 .

Spectral lags

There are a number of redshift indicators that can be used for GRBs without spectroscopic redshift measurements. One such indicator is the spectral lag which combines the spectral and temporal properties of the prompt GRB emission. The spectral lag is a measure of the time delay between GRB emission in a high-energy γ -ray band relative to the arrival of photons in a low-energy band. The typical lag values measured for long-duration

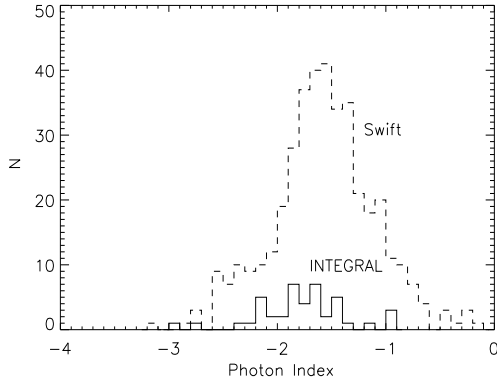


FIGURE 7. Power-law photon index distributions for INTEGRAL (solid line) and Swift (dashed line). The Swift data for 395 GRBs is taken from http://swift.gsfc.nasa.gov/docs/swift/archive/grb_table.html.

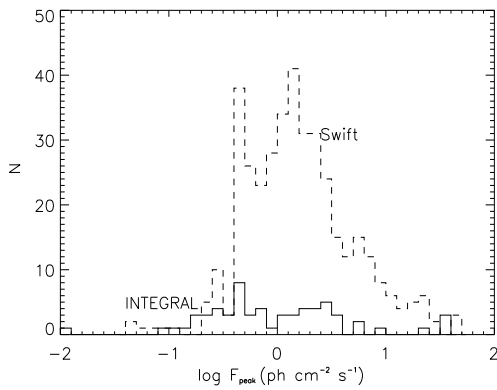


FIGURE 8. Peak flux distribution for GRBs detected by INTEGRAL (20–200 keV, solid line) and Swift (15–150 keV, dashed line). The Swift data for 388 GRBs is taken from http://swift.gsfc.nasa.gov/docs/swift/archive/grb_table.html.

GRBs detected by the Burst and Transient Source Experiment (BATSE) between the 25–50 keV and 100–300 keV channels concentrate at ~ 100 ms [71]. An anticorrelation between spectral lag and isotropic peak luminosity was first observed by Norris et al. [71], using 6 BATSE bursts with measured redshifts. However, there exist notable outliers, in particular the ultra-low luminosity bursts GRB 980425, GRB 031203 and GRB 060218, associated with the supernovae SN 1998bw, SN 2003lw and SN 2006aj, respectively.

In order to measure the lags of INTEGRAL GRBs, background-subtracted lightcurves were extracted in 25–50 keV and 50–300 keV energy bands. The lag, τ , between two energy channels was determined by computing the cross-correlation function (CCF) between the two

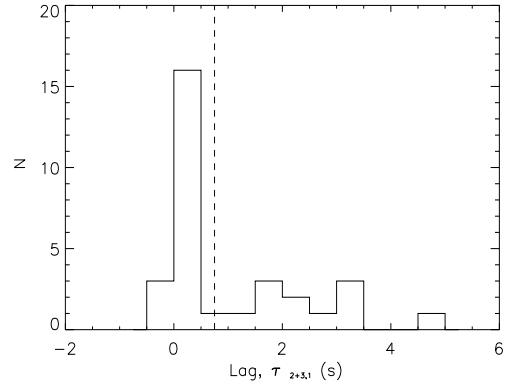


FIGURE 9. Spectral lag distribution for the 30 INTEGRAL GRBs for which a lag could be measured between 25–50 keV and 50–300 keV. The distribution is separated by the dashed line into short-lag and long-lag GRBs at $\tau=0.75$ s.

lightcurves as a function of temporal lag as described by Band [72] and Norris et al. [71]. Assuming the time profiles in both energy channels display sufficient similarity, the peak in the CCF then corresponds to the time lag of the GRB between the two energy channels in question.

The number distribution of spectral lags is given in Fig. 9 for the 30 long-duration GRBs with a measured lag between 25–50 keV and 50–300 keV. No statistically significant negative spectral lags are found. A long tail extending to ~ 5 s is observed in the lag distribution in Fig. 9 and a clear separation between short and long lag is drawn at $\tau \sim 0.75$ s. Thus, long-lag bursts have $\tau > 0.75$ s and those with $\tau < 0.75$ s are referred to as short-lag GRBs. There are 12 long-lag GRBs in the INTEGRAL sample.

The logN-logP distribution is given in Fig. 10 for all IBIS GRBs and separately for the subset of 12 long-lag GRBs. The distribution is biased by the lower sensitivity of IBIS at large off-axis angles. However, the long-lag GRBs appear to form a separate population at low peak fluxes.

Spatial distribution in Supergalactic coordinates

The INTEGRAL exposure map and distribution of GRBs in supergalactic coordinates is shown in Fig. 11. All of the INTEGRAL GRBs are divided almost equally between the half of the sky above and below $\pm 30^\circ$, in agreement with the exposure map which has $\sim 52\%$ of the exposure time within $\pm 30^\circ$ of the supergalactic plane. However, 10 of the 12 long-lag GRBs are concentrated at supergalactic latitudes between $\pm 30^\circ$. The

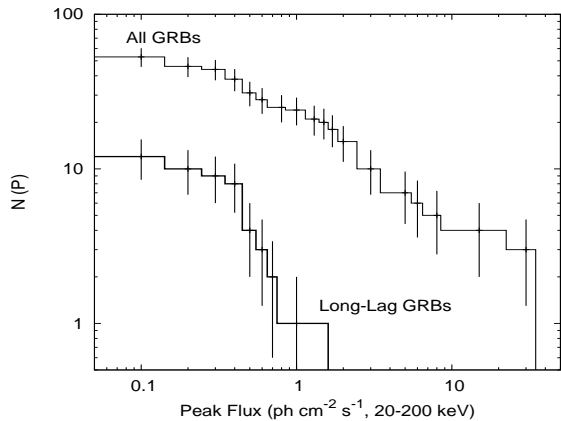


FIGURE 10. The cumulative log N-log P distribution of the GRBs detected by IBIS, with peak flux, P, measured between 20–200 keV. The small subset of 12 long-lag GRBs is shown separately.

quadrupole moment [73] has a value of $Q = -0.166 \pm 0.086$ for the long-lag GRBs and indicates an anisotropy in the distribution of these GRBs with respect to the supergalactic plane. This result leads us to conclude that long-lag GRBs may trace the features of the nearby large-scale structure of the Universe and is a further indication that most long-lag GRBs are nearby and have low luminosity.

A nearby population of long-lag, low-luminosity GRBs has previously been proposed based on the detections of GRB 980425 and XRF 060218 [e.g. 74]. The distance to the long-lag GRBs can also be constrained by association and comparison with the two low luminosity bursts GRB 980425 ($\tau \sim 2.8$ s) and XRF 060218 ($\tau \sim 60$ s) which would have been detected in the fully-coded field of view of IBIS to 135 Mpc and 290 Mpc, respectively. The association of the long-lag GRBs with known low luminosity GRBs and with the supergalactic plane implies that they are at similar distances. It has also been pointed out that weak BATSE GRBs appear to be correlated with galaxies out to distances of ~ 155 Mpc [75].

GRBs have a long lag when a typical value of 0.1 s is redshifted by a large factor or alternatively it is an intrinsic property of a low-luminosity GRB such as GRB 980425 and XRF 060218. The rate of $z > 5$ GRBs in IBIS has been modelled [e.g. 76] and is unlikely to be more than 1 or 2 GRBs in 5 years of observations. We evaluate the rate of such GRBs over the whole sky using the 8 long-lag *INTEGRAL* GRBs in the partially-coded field of view of IBIS at 50% coding (0.1 sr) over an exposure time of 4 years, adopting a distance of 250 Mpc and assuming that 2 of the 8 GRBs are at high redshift. We obtain $2640 \text{ Gpc}^{-3} \text{ yr}^{-1}$, in which the major

uncertainty is the distance. The rate of low-luminosity GRBs at the adopted distance of 250 Mpc exceeds the upper limit of $< 300 \text{ Gpc}^{-3} \text{ yr}^{-1}$ of Type Ib/c SN producing GRBs, which was derived assuming that all low luminosity GRBs would produce a SN and be as radio bright as the SN GRBs [77]. However, the low luminosity GRB 060605 has no associated SN to faint limits and is evidence for a quiet end for some massive stars [e.g. 78].

The association of low luminosity GRBs with the supergalactic plane is not proof that they are associated with clusters of galaxies but indicates that clusters may play a role. It is interesting to note that the rate of Type Ia SNe is higher in elliptical galaxies in clusters than in field ellipticals by a factor of ~ 3 [79]. This effect is due to galaxy-galaxy interactions which can affect the evolution and properties of binary systems. In this case, there should also be an increase in the merger rate of white dwarfs or a white dwarf with a neutron star or black hole. A merger involving a white dwarf [e.g. 80] should produce a long GRB that is likely to be fainter than the formation of a black hole in cosmological GRBs. There will be no supernova in the merger of a white dwarf with a neutron star or black hole, and probably a faint afterglow.

CONCLUSION

INTEGRAL is an Observatory type Gamma-ray mission with two main instruments optimized for high resolution γ -ray imaging and spectroscopy in the energy range from 15 keV up to 10 MeV.

The observatory, even if not fully optimized for GRB science (mainly due to on-board limited resources in term of TLM, buffering memory and computing power etc.) features a substantially large field of view of the main instruments (> 1000 squared degrees), real time photon by photon transmission to ground, and the IBAS system that distributes the position of the GRB very effectively, with an accuracy of the order of 1 to 3 arcmin a few seconds after the onset of the burst.

From its launch in October 2002 to date, *INTEGRAL* has detected and localised 65 GRBs. They have provided significant insight into the prompt γ -ray emission in the hard-X/soft- γ -ray energy range, i.e. where GRBs emit a large fraction of their energy. Furthermore, *INTEGRAL* provides unique sensitivity in the MeV range via the IBIS Compton mode, an energy region which was not sensitively covered by other operative satellites until the recent launches of *AGILE* and *FERMI*. Also, for the brightest bursts, both IBIS and SPI have independent, moderate, polarization capabilities.

Due to the limited FoV the overall rate of accurately positioned GRBs is limited to about 0.8 GRBs per month, with real time localisations enabling multi-

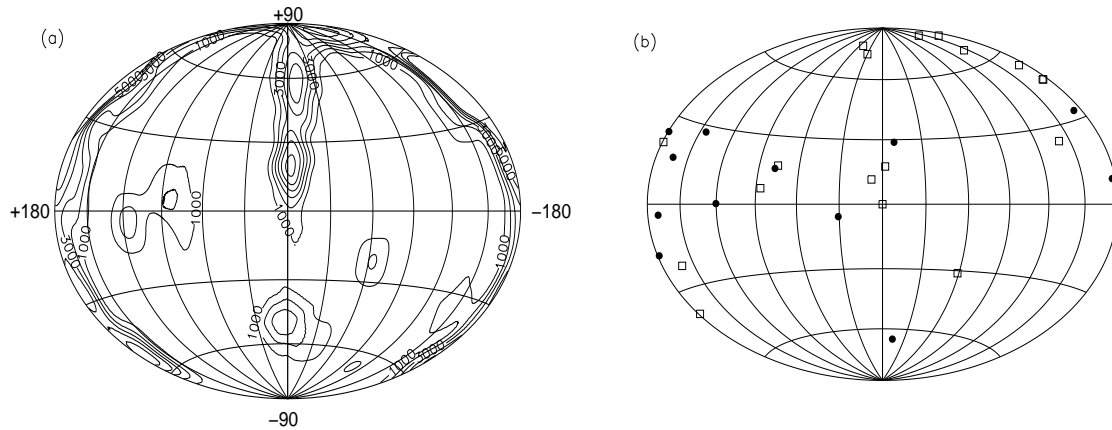


FIGURE 11. **a** INTEGRAL exposure map in supergalactic coordinates (contours in units of kiloseconds). **b** The distribution of INTEGRAL GRBs in supergalactic coordinates; the open squares represent short-lag GRBs ($\tau < 0.75$ s) and filled circles those GRBs with long lags ($\tau > 0.75$ s).

wavelength observations to be carried out by other space-based missions and ground-based telescopes. On the other hand, when compared with SWIFT, a GRB oriented mission, INTEGRAL detects proportionally more faint GRBs due to its narrower FoV that limits the count rate due X-Ray Diffuse Background, which is the limiting factor to sensitivity in the lower operative energy range ($E < 100 - 150$ keV). The sensitivity of IBIS is such that it can detect very faint GRBs, allowing the investigation of the population of low-luminosity GRBs with long lags which appears to be a low-luminosity population distinct from the high-luminosity one and is inferred to be local. Finally, the all-sky rate of GRBs with a flux above $0.15 \text{ ph cm}^{-2} \text{ s}^{-1}$ is 1400 yr^{-1} , based on the bursts detected in the IBIS fully coded field of view.

After almost 7 years of successful operation in orbit, the European Space Agency is in the process of extending INTEGRAL operations beyond 2012. INTEGRAL has all the redundant system still unused, all of the on board systems perfectly operative, including the two main instruments and monitors. The mission's extension will enable us to collect several tens of new GRBs, in turn allowing us to confirm with higher statistical confidence the local nature of the long lag ones.

We believe it is mandatory to maintain INTEGRAL in operation as an important space observatory open to the community at large, operating in full synergy with XMM, CHANDRA, Suzaku, RXTE and SWIFT for the low energy part of the X-ray domain, and AGILE and FERMI for the γ -ray range.

The impressive space satellite fleet now available to the scientific community has resulted in the present golden age for high energy astrophysical science, while anticipating the the new generation of γ -ray flight missions such as EXIST, etc.

ACKNOWLEDGMENTS

PU and AB acknowledge financial contribution from ASI-INAF contract I/008/07/0. AC is grateful to the Italian L'Oreal-UNESCO program "For Women in Science" and acknowledges the support of ASI-INAF contract I/088/06/0.

REFERENCES

1. A. Bird, et al., *in preparation* (2009).
2. C. Winkler, et al., *A&A* **411**, L1 (2003).
3. P. Ubertini, et al., *A&A* **411**, L131 (2003).
4. G. Vedrenne, et al., *A&A* **411**, L63 (2003).
5. N. Lund, et al., *A&A* **411**, L231 (2003).
6. M. Mass-Hesse, et al., *A&A* **411**, L261 (2003).
7. G. Skinner, and P. Connell, *A&A* **411**, L123 (2003).
8. T. Courvoisier, et al., *A&A* **411**, L49 (2003).
9. G. Di Cocco, et al., *A&A* **411**, L189 (2003).
10. A. Bazzano, and A. Paizis, *GCN* **1706** (2002).
11. G. Malaguti, et al., *A&A* **411**, L307 (2003).
12. K. Hurley, et al., *GCN* **1709** (2002).
13. S. Mereghetti, et al., *Proc. of the 4th INTEGRAL Workshop ESA-SP* **459**, 513 (2001).
14. D. Götz, et al., *A&A* **409**, 831 (2003).
15. R. D. Preece, et al., *ApJ* **506**, L23 (1998).
16. L. A. Ford, et al., *ApJ* **439**, 307 (1995).
17. F. Frontera, et al., *ApJS* **127**, 59 (2000).
18. R. Marcinkowski, et al., *A&A* **452**, 113 (2006).
19. K. Hurley, et al., *GCN* **2127**, 1 (2003).
20. R. D. Preece, et al., *ApJS* **126**, 19 (2000).
21. J. I. Katz, et al., *ApJ* **432**, L107 (1994).
22. M. Tavani, et al., *Ap&SS* **231**, 181 (1995).
23. M. V. Medvedev, et al., *ApJ* **540**, 704 (2000).
24. G. Ghirlanda, et al., *A&A* **406**, 879 (2003).
25. R. S. Mallozzi, et al., *ApJ* **454**, 597 (1995).
26. L. Amati, et al., *A&A* **390**, 81 (2002).
27. G. Ghirlanda, et al., *ApJ* **616**, 331 (2004).
28. D. Gotz, et al., *GCN* **2640** (2004).

29. D. Band, et al., *ApJ* **413**, 281 (1993).
30. S. Campana, and A. Moretti, *GCN* **2649** (2004).
31. S. Campana, et al., *GCN* **2656** (2004).
32. P. D'Avanzo, et al., *Nuovo Cimento B* **121**, 1467 (2006).
33. G. Stratta, et al., *A&A* **461**, 485 (2007).
34. L. Amati, et al., *MNRAS* **391**, 577–584 (2008).
35. S. Mereghetti, et al., *ApJ* **590**, L73 (2003).
36. W. S. Paciesas, et al., *ApJS* **122**, 465 (1999).
37. R. Protassov, et al., *ApJ* **571**, 545 (2002).
38. L. Piro, et al., *ApJ* **514**, 73 (1999).
39. L. Piro, et al., *A&AS* **138**, 431 (1999).
40. L. A. Antonelli, et al., *ApJ* **545**, 39 (2000).
41. L. Amati, et al., *Science* **290**, 953 (2000).
42. L. Piro, et al., *Science* **290**, 955 (2000).
43. R. Protassov, et al., *AAS* **197**, 1604 (2000).
44. A. Yoshida, et al., *ApJ* **557**, 27 (2001).
45. R. Watson, et al., *ApJ* **595**, 29 (2003).
46. A. J. Castro-Tirado, et al., *A&A* **411**, L315 (2003).
47. F. Harrison, et al., *ApJ* **559**, 123 (1999).
48. J. J. in't Zand, et al., *ApJ* **559**, 710 (2001).
49. A. Corsi, et al., *A&A* **438**, 829 (2005).
50. S. Y. Sazonov, A. A. Lutovinov, and R. A. Sunyaev, *Nature* **430**, 646–648 (2004).
51. G. Ghisellini, G. Ghirlanda, S. Mereghetti, et al., *MNRAS* **372**, 1699–1709 (2006).
52. K. Toma, et al., *ApJ*, to appear in (*arXiv:0812.2483*) (2008).
53. S. McGlynn, et al., *A&A* **466**, 895 (2007).
54. D. Götz, et al., *GCN* **2866** (2004).
55. S. Barthelmy, et al., *GCN* **2874** (2004).
56. S. MacBreen, et al., *A&A* **455**, 433 (2006).
57. E. Fenimore, et al., *GCN* **2906** (2004).
58. A. M. Levine, et al., *ApJL* **469**, L33 (2004).
59. A. Levine, et al., *GCN* **2917**, 1 (2004).
60. E. Kalemici, et al., *ApJS* **169**, 75 (2007).
61. D. Götz, et al., *ApJ* **695**, 208 (2009).
62. F. Lei, et al., *Space Sci. Rev.* **82**, 309 (1997).
63. J. Granot, et al., *ApJ* **596**, L17 (2003).
64. J. Granot, and A. Königl, *ApJ* **594**, L83 (2003).
65. E. Nakar, et al., *J. Cosmol. Astropart. Phys.* **10**, 005 (2003).
66. M. Lyutikov, et al., *ApJ* **597**, 998 (2003).
67. G. Ghisellini, et al., *MNRAS* **309**, L7 (1999).
68. E. Waxman, et al., *Nature* **423**, 388 (2003).
69. D. Lazzati, et al., *MNRAS* **347**, L1 (2004).
70. C. Kouveliotou, C. A. Meegan, G. J. Fishman, et al., *ApJL* **413**, L101–L104 (1993).
71. J. P. Norris, G. F. Marani, and J. T. Bonnell, *ApJ* **534**, 248–257 (2000).
72. D. L. Band, *ApJ* **486**, 928 (1997).
73. D. H. Hartmann, M. S. Briggs, and K. Mannheim, “Search for Supergalactic Anisotropies in the 3B Catalog,” in *American Institute of Physics Conference Series*, 1996, vol. 384, p. 397.
74. D. Guetta, R. Perna, L. Stella, and M. Vietri, *ApJL* **615**, L73–L76 (2004).
75. R. Chapman, N. R. Tanvir, R. S. Priddey, and A. J. Levan, *MNRAS* **382**, L21–L25 (2007).
76. J. Gorosabel, N. Lund, S. Brandt, N. J. Westergaard, and J. M. Castro Cerón, *A&A* **427**, 87–93 (2004).
77. A. M. Soderberg, S. R. Kulkarni, E. Nakar, et al., *Nature* **442**, 1014–1017 (2006).
78. J. P. U. Fynbo, D. Watson, C. C. Thöne, et al., *Nature* **444**, 1047–1049 (2006).
79. F. Mannucci, D. Maoz, K. Sharon, et al., *MNRAS* p. 1132 (2007).
80. A. King, E. Olsson, and M. B. Davies, *MNRAS* **374**, L34–L36 (2007).